ACS ENGINEERING Au
AN OPEN ACCESS JOURNAL OF THE AMERICAN CHEMICAL SOCIETY

pubs.acs.org/engineeringau

Article

Bifunctional Pt–Re Catalysts in Hydrodeoxygenation of Isoeugenol as a Model Compound for Renewable Jet Fuel Production

Mark Martinez-Klimov, Päivi Mäki-Arvela, Ayşegül Çiftçi, Narendra Kumar, Kari Eränen, Markus Peurla, Emiel J. M. Hensen, and Dmitry Yu. Murzin*

Cite This: *ACS Eng. Au* 2022, 2, 436–449

Read Online

ACCESS | Metrics & More | Article Recommendations

ABSTRACT: Bimetallic platinum–rhenium catalysts supported on activated carbon were tested for the hydrodeoxygenation (HDO) of isoeugenol at 250 °C and 30 bar of H_2 in a batch reactor. The catalysts were characterized by inductively coupled plasma atomic emission spectrometry (ICP-IES), N_2 physisorption, electron microscopy (high-angle annular dark-field scanning transmission electron microscopy (HAADF-STEM), transmission electron microscopy (TEM)), temperature-programmed reduction, X-ray absorption spectroscopy (X-ray absorption near-edge structure (XANES) and extended X-ray absorption fine structure (EXAFS)), and temperature-programmed desorption of ammonia. Bimetallic catalysts containing Pt and Re were much more active than monometallic Pt/C and Re/C. Complete isoeugenol conversion, high propylcyclohexane yield (99%), and a high liquid-phase mass balance (77%) were obtained for the catalyst with the highest Re loading, Pt–Re(1:5)/C. Such high activity is attributed to a synergistic effect between the reduced Pt and the Re-oxide species, as both metal active sites and oxygen vacancies are required for HDO. The apparent activation energy for the HDO of isoeugenol with Pt–Re(1:5)/C was 44 kJ/mol.

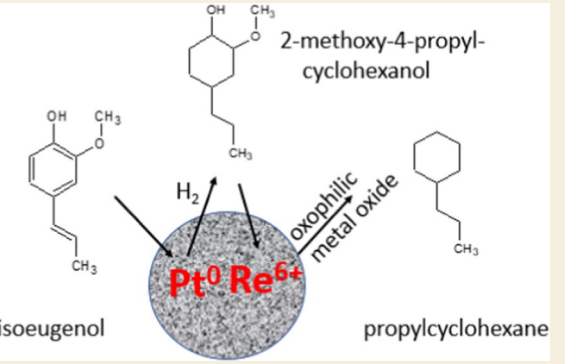

KEYWORDS: *hydrodeoxygenation, bimetallic catalyst, platinum, rhenium, activated carbon, jet fuel*

INTRODUCTION

Depleting fossil resources and increased greenhouse gas emissions have accelerated the development of alternative processes and technologies assisting the transition to the use of renewable fuels.[1] These can for instance be obtained from biomass, an abundant resource comprised of cellulose, commonly used in the pulp and paper industry,[2] hemicellulose, already employed to produce platform chemicals like xylitol[3] and furfural,[4] and lignin, which can be upgraded to produce fine chemicals and biofuels.[5,6]

Lignin is of particular interest, as it is one of the main natural sources containing aromatic rings.[7] Obtained as an undesired residue from industries like paper making, it can be utilized to obtain valuable products.[8] Lignin is a complex biopolymer, which can be depolymerized through thermochemical processes into a mixture of oxygenated molecules.[9] Lignin-derived mixtures need to be further upgraded, as they exhibit a low heating value, and are also viscous and corrosive because of their oxygen content.[10]

A common way to remove oxygen-containing functionalities from these molecules is hydrodeoxygenation (HDO). Catalysts used for HDO of biogenic compounds are often bifunctional, as they require a metal for hydrogenation and a solid acid support or a metal oxide with O-vacancies.[11,12] Studies on HDO catalysts were initially performed with sulfided NiMo and CoMo supported on Al_2O_3 and SiO_2 used for hydrodesulfurization (HDS) due to obvious similarities between HDO and HDS.[13] Recently, attention has shifted to non-sulfided monometallic and bimetallic catalysts on a variety of supports, such as different types of carbon (activated carbon,[14] carbon black,[15] Vulcan carbon),[16] Sibunit,[17] metal oxides (TiO_2,[18] ZrO_2,[19] CeO_2),[2020] and nanostructured materials (carbon nanotubes,[21] SBA-15,[22] and MCM-41).[23] The most studied metals for HDO include Ni, Mo, Co, Pt, Ru, and Pd.[24]

Bimetallic Pt–Re catalysts have been widely used in reforming processes[25] because Re has a promoting effect on such catalysts, improving activity and stability.[26] The use of Re is not only limited to reforming, as it is also used in fuel cells and other sustainable processes.[27] This combination of metals, however, has been scarcely used for HDO of isoeugenol. Our previous study on bimetallic Pt–Re catalysts supported on a

Received: March 16, 2022
Revised: May 11, 2022
Accepted: May 12, 2022
Published: June 2, 2022

https://doi.org/10.1021/acsengineeringau.2c00015
ACS Eng. Au 2022, 2, 436–449

mesoporous carbon (Sibunit) demonstrated an increased activity when compared to typical catalysts reported in the literature and used under similar reaction conditions.[17] The previous investigation was limited regarding the effect of Re on isoeugenol HDO, as only three bimetallic catalysts with less variations of Pt and Re loadings were tested.

Activated carbon is the most common carbon support used in catalysis. It is attractive due to its large surface area and porosity, allowing for better dispersion of the active phase.[28] Due to its hydrophobicity, activated carbon shows a particular affinity to nonpolar solvents, such as hydrocarbons.[29] Other advantages include the easier reducibility of supported metals and the recovery of these metals by burning away the support.[30]

HDO of model molecules representing lignin phenolics is often studied to obtain an insight into catalytic activity and stability. Phenol,[31] guaiacol,[32,33] anisole,[22] and vanillin[34] are the most common model molecules studied due to their availability and simplicity, although they are not the most representative of real lignin feedstock.[35] Isoeugenol is an attractive lignin-derived model compound, as it closely resembles the monomeric phenylpropane building blocks found in lignin. It contains methoxy, hydroxyl, and allyl groups, which are functional groups commonly found in most lignin-derived compounds.[36] The main HDO product of isoeugenol is propylcyclohexane, a molecule that can be representative of the hydrocarbons found in jet fuel.

Renewable jet fuel must exhibit similar properties as conventional jet fuel to be used with current technologies. Fossil-derived jet fuel consists mainly of aliphatic and aromatic hydrocarbons in the range of C_8−C_{16}, with alkanes, alkenes, cycloalkanes, and aromatics being the main components.[37,38]

The need for renewable jet fuel arises as new regulations aim to boost sustainable fuels and meet climate targets.[39] More importantly, hydrocarbons used for commercial aircrafts cannot be replaced by batteries, i.e., the direction the automobile industry seems to be taking, as batteries with enough energy density to propel a plane would be too heavy.[40]

However, a transition toward renewable and sustainable fuels could be done with the utilization of biomass and oxygen removal processes such as HDO. Hydrocarbons obtained from HDO of lignocellulosic biomass could potentially be mixed with fossil-derived hydrocarbons or even replace them, helping to lower the carbon footprint.[41]

In the present work, hydrodeoxygenation of isoeugenol over bimetallic Pt−Re catalysts supported on activated carbon was studied and compared to monometallic Pt and Re catalysts. To study the effect of Re on the bimetallic catalytic systems and their activity in HDO, a series of catalysts with a fixed amount of Pt and varied Re loading were investigated.

EXPERIMENTAL SECTION

Catalyst preparation and the following characterization techniques; inductively coupled plasma atomic emission spectrometry (ICP-IES), high-angle annular dark-field scanning transmission electron microscopy (HAADF-STEM), temperature-programmed reduction (TPR), X-ray absorption spectroscopy (XAS), and temperature-programmed desorption of ammonia (TPD-NH_3) have been reported in a previous publication.[26]

Catalyst Preparation

The catalysts were prepared by incipient wetness impregnation of the dissolved metal precursors chloroplatinic acid hexahydrate ($H_2PtCl_6 \cdot 6H_2O$) and perrhenic acid ($HReO_4$, Aldrich, 65−70 wt % in H_2O, 99.99%) onto activated carbon (NORIT RX3 EXTRA). Bimetallic catalysts supported on carbon were denoted as PRC*XX*, where PR corresponds to platinum and rhenium, C corresponds to the carbon support, and *XX* to the molar ratio. For bimetallic catalysts, the molar ratios of Pt/Re were set to 1:1, 2:1, 1:2, and 1:5 by maintaining Pt loading to 2.5 wt % and varying the Re loading accordingly.

Monometallic catalysts Pt/C and Re/C were also studied, their respective nominal loading was 2.5 wt % for both Pt and Re.

Preparation of Pt and Pt−Re catalysts supported on carbon was as follows: activated carbon was first dried overnight at 110 °C, followed by impregnation of the dissolved Pt precursor ($H_2PtCl_6 \cdot 6H_2O$) in deionized water. The catalyst was left to dry overnight at 110 °C. For bimetallic Pt−Re catalysts, subsequent impregnation of the Re precursor ($HReO_4$) was performed, followed by drying overnight at 110 °C.

Monometallic Re/C was prepared by the same method, only using the Re precursor.[26]

A summary of the catalysts used in the current work is presented in Table 1.

Table 1. Summary of Catalysts Supported on Activated Carbon Used for HDO of Isoeugenol

		nominal metal loading (wt %)		
catalyst denomination	metal	Pt	Re	metal molar ratio
Pt/C	platinum	2.5		
Re/C	rhenium		2.4	
PRC21	platinum, rhenium	2.5	1.2	2:1
PRC11	platinum, rhenium	2.5	2.4	1:1
PRC12	platinum, rhenium	2.5	4.8	1:2
PRC15	platinum, rhenium	2.5	11.9	1:5

Catalytic Tests

Prior to the experiments, the catalysts were reduced *ex situ* in a U-shaped reactor, under a hydrogen flow (40 mL/min) at 350 °C for 180 min, with a heating ramp of 10 °C/min. After reduction was finished, the system was flushed with argon, and dodecane was added to avoid reoxidation.

HDO reactions were carried out in a 300 mL stainless steel batch reactor (PARR) equipped with a heating jacket and mechanical stirring. A heating rate of the reactor was 10 °C/min. To avoid external mass-transfer limitations, the stirring speed was set to 900 rpm. To avoid internal mass-transfer limitations, the size of the catalyst particles was below 63 μm. The following quantities were used for the reaction: 0.1 g of the reactant, 0.05 g of the catalyst, and 50 mL of dodecane.

The reactor was initially purged with 7 bar of argon (AGA, 99.999%) for 10 min, followed by purging with 10 bar of hydrogen (AGA, 99.999%) for 10 min. The reactor was then pressurized to 20 bar with hydrogen. After heating to the reaction temperature, hydrogen was added to the reactor to reach 30 bar of total pressure if needed.

Reaction time started after the reaction temperature and stirring speed were reached. Samples were taken at regular time intervals and analyzed by GC and GC/MS. A DB-1 capillary column (Agilent 122-103e) of 30 m length, 250 μm internal diameter, and 0.5 μm film thickness was utilized for GC analysis. The carrier gas employed was He (flow rate of 1.7 mL/min). The temperature program was 60 °C (5 min), 3 °C/min to 135 °C, and 15 °C/min to 300 °C. GC−MS analysis was performed using the same temperature program and type of column as used in GC.

Catalyst Characterization

Inductively Coupled Plasma Atomic Emission Spectrometry (ICP-IES). Elemental analysis was performed with inductively coupled plasma atomic emission spectrometry (ICP-AES). Determination of

https://doi.org/10.1021/acsengineeringau.2c00015
ACS Eng. Au 2022, 2, 436−449

Table 2. Metal Loading and Textural Properties of the Catalysts

	metal loading (wt %)[26]			textural characteristics			
catalyst	Pt	Re	molar ratio Pt/Re	SSA (m^2/g)	V_Σ (cm^3/g)	V_{MP} (cm^3/g)	D_P (nm)
C support				1096	0.57	0.47	0.59, 0.67
Pt/C	2.44			1033	0.47	0.37	0.59, 0.67
Re/C		2.78		1030	0.49	0.39	0.59, 0.67
PRC21	2.48	1.53	2:1.2	1026	0.49	0.40	0.59, 0.68
PRC11	2.53	2.86	1:1.2	1019	0.47	0.38	0.59, 0.67
PRC12	2.51	5.58	1:2.3	1017	0.48	0.37	0.59, 0.67
PRC15	2.28	13.41	1:6	1014	0.48	0.36	0.59, 0.68
PRC11 spent				1002	0.43	0.35	0.59, 0.68
PRC21 spent				1005	0.43	0.35	0.59, 0.68
PRC15 spent (270 °C)				992	0.39	0.33	0.59, 0.68

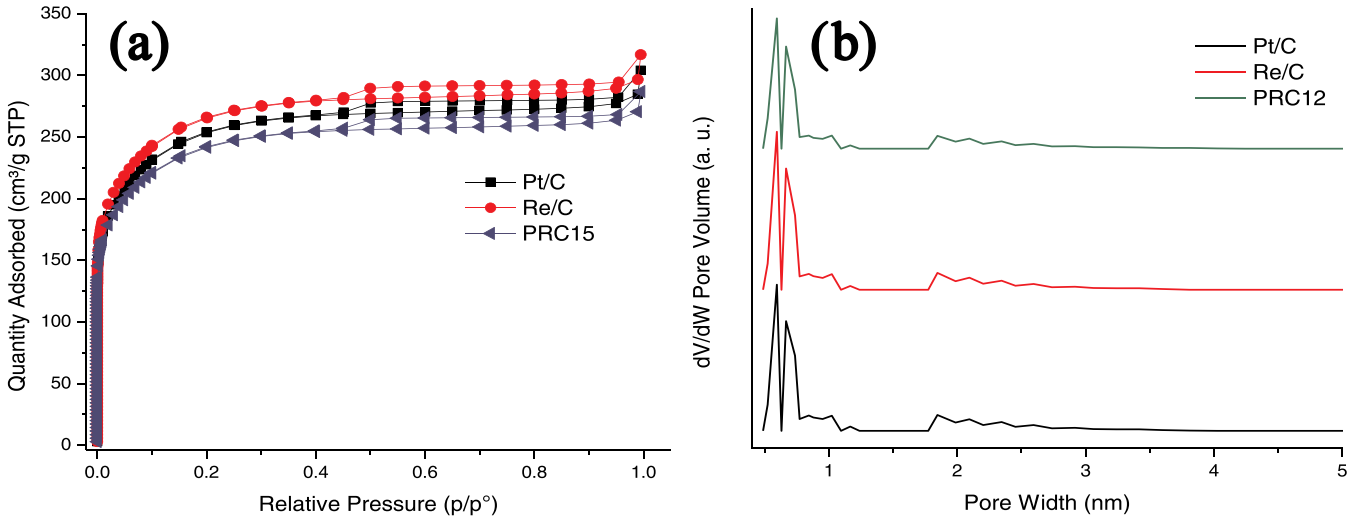

Figure 1. (a) Adsorption−desorption isotherm and (b) pore-size distribution of Pt/C, Re/C, and PRC12.

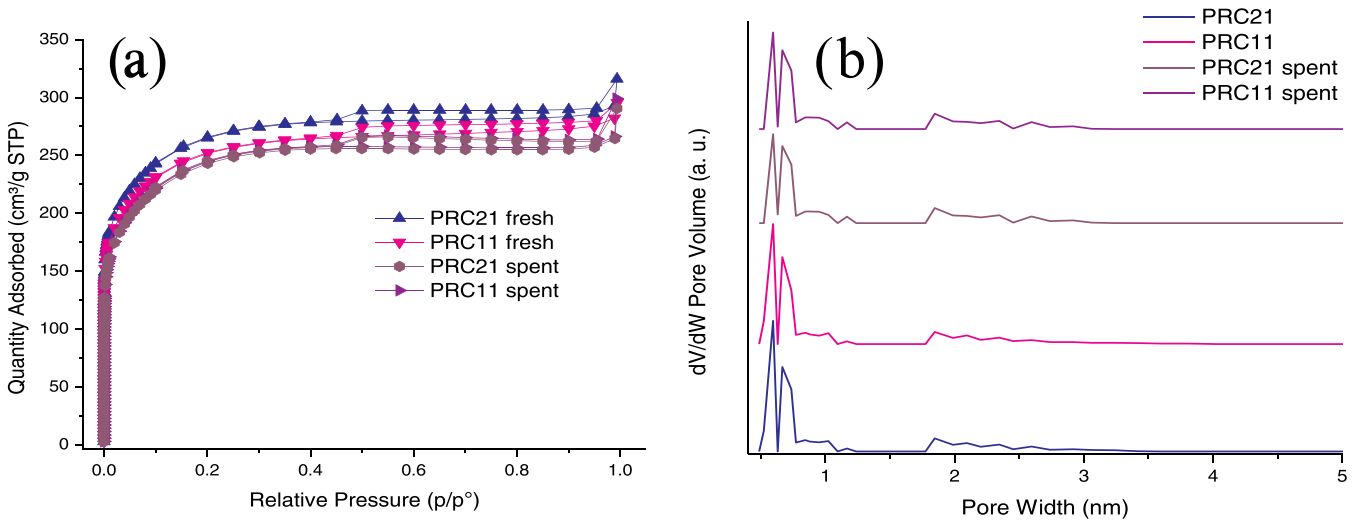

Figure 2. (a) Nitrogen adsorption−desorption isotherms and (b) pore-size distribution comparison of fresh and spent catalysts.

the metal loading of the catalysts was performed on a Goffin Meyvis Spectro Cirusccd apparatus.[26]

Nitrogen Physisorption. Textural properties of the fresh and spent catalysts were determined by nitrogen physisorption (Micrometrics 3Flex-3500). The specific surface area was determined by the Dubinin−Radushkevich method and pore-size distributions were calculated with the density functional theory (DFT) method. The catalyst pretreatment consisted of two stages of outgassing. First, they were outgassed *ex situ* in a Micromeritics VacPrep 061 Sample Degas system under vacuum at 200 °C for 20−24 h, followed by *in situ* degassing for 5 h at 250 °C.

Electron Microscopy (HAADF-STEM, TEM). Electron microscopy was utilized to determine the metal particle sizes and evaluate the metal dispersion. High-angle annular dark-field scanning transmission electron microscopy (HAADF-STEM) micrographs were obtained at room temperature on a CryoTitan transmission electron

https://doi.org/10.1021/acsengineeringau.2c00015
ACS Eng. Au 2022, 2, 436−449

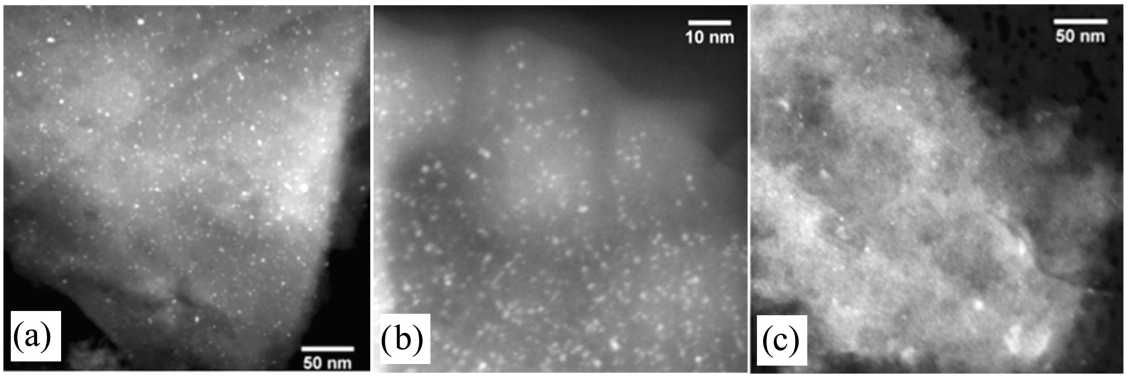

Figure 3. HAADF-STEM micrographs of fresh (a) Pt/C, (b) PRC11, and (c) PRC15 catalysts. Reprinted with permission from ref 26. Copyright 2014 Elsevier.

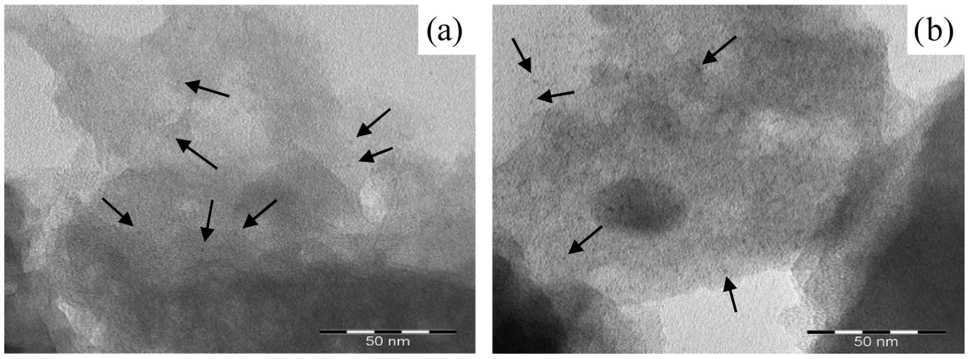

Figure 4. TEM micrographs of the spent (a) PRC11 and (b) PRC15 (270 °C) with arrows pointing at metallic particles.

microscope equipped with a field emission gun (FEG) and a Cryo-TWIN objective lens. STEM images were acquired with a Fishione HAADF detector.[26] The spent catalysts were characterized with a JEM-1400Plus (JEOL, Japan) transmission electron microscope at 120 kV maximal acceleration voltage. The samples were reduced, ground, and suspended in ethanol and then mounted on a copper grid prior to the analysis. The average particle size was determined by measuring the diameter of more than 300 particles.

Temperature-Programmed Reduction (TPR). TPR analysis was performed using a tubular quartz reactor and a thermal conductivity detector (TCD). The sample was reduced in 4 vol % H_2 in N_2 at a flow rate of 8 mL/min. The heating was carried out from room temperature until 800 °C with a heating rate of 10 °C/min. The H_2 signal was calibrated using a reference catalyst (CuO/SiO_2).[26]

X-Ray Photoelectron Spectroscopy (XPS). X-ray photoelectron spectroscopy (XPS) measurements were performed *ex situ* with a Nexsa XPS (ESCA) photoelectron spectrometer manufactured by Thermo Scientific, using a monochromated Al Kα excitation source. The catalysts were reduced *ex situ* and then placed on a sample holder for analysis.

X-Ray Absorption Spectroscopy (XAS). XAS was carried out at the European Synchrotron Radiation Facility (ESRF) in Grenoble, France (storage ring 6.0 GeV, ring current 200 mA). Data were collected in transmission mode for Pt LIII and Re LIII edges using a double crystal Si(111) monochromator solid-state detector. EXAFS was performed with an EXCURVE931 using curved wave theory. Pt foil was used for calibration. For the Re LIII edge, Re powder, and NH_4ReO_4 were used as the reference. The spectra were recorded in a stainless steel cell under a He and H_2 atmosphere. XANES spectra were recorded while heating the sample to 550 °C at a rate of 10 °C/min. EXAFS spectra were obtained after the sample was cooled.[26]

Temperature-Programmed Desorption of Ammonia (TPD-NH_3). Temperature-programmed desorption (TPD) of ammonia was performed in a tubular quartz reactor attached to a heating oven and coupled to a quadrupole mass spectrometer (Balzers TPG-300). The samples were pre-reduced *in situ* prior to the analysis. Afterward, the catalyst was exposed to pure NH_3 at room temperature. The temperature ramp used for the analysis was 10 °C/min under He flow (50 mL/min). Signals corresponding to He, NH_3, and H_2O were recorded simultaneously.[26]

RESULTS AND DISCUSSION

Catalyst Characterization

A summary of the metal loading and textural properties of the catalysts is presented in Table 2.

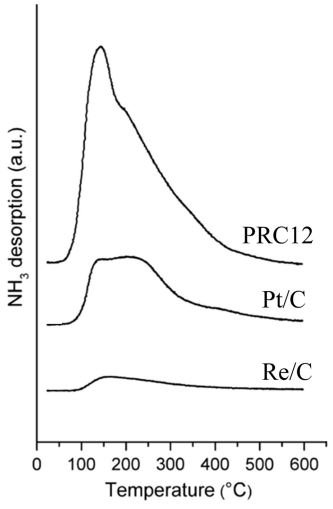

Figure 5. NH_3-TPD profiles of Pt/C, Re/C, and PRC12. Reprinted with permission from ref 26. Copyright 2014 Elsevier.

https://doi.org/10.1021/acsengineeringau.2c00015
ACS Eng. Au 2022, 2, 436−449

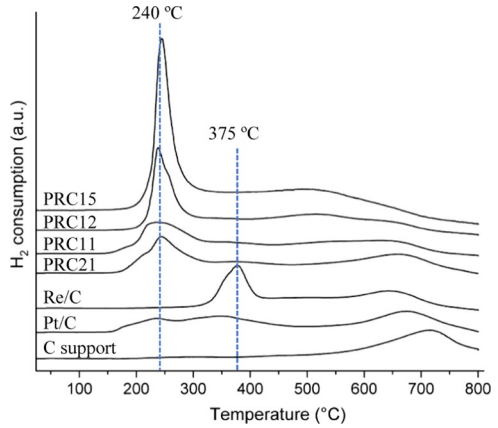

Figure 6. TPR profiles of the activated carbon support, monometallic Pt/C and (c) Re/C and bimetallic PRC21, PRC11, PRC12 and PRC15 catalysts. Reprinted with permission from ref 26. Copyright 2014 Elsevier.

Table 3. Temperature-Programmed Reduction (TPR) Results for Mono- and Bimetallic Catalysts

catalyst	T_{max} (°C)	H_2/M ratio[26]
Pt/C	240	4.84
Re/C	375	9.59
PRC21	240	6.40
PRC11	240	4.70
PRC12	240	3.62
PRC15	240	3.55

The catalysts displayed attractive characteristics; metal atomic ratios (Table 2) calculated by the metal loadings obtained by ICP were close to the nominal values, indicating good deposition. Additionally, nitrogen physisorption results (Table 2) showed a high specific surface (SSA) area for all catalysts (ca. 1000 m^2/g). Catalysts displayed a slight decrease in textural properties when compared to the pure carbon support, which could be caused by metal deposition. The highest SSA, total pore volume (V_Σ), and the micropore volume (V_{MP}) were obtained for monometallic Pt/C and Re/C catalysts, while bimetallic catalysts exhibited a slight decrease in the textural properties, which could be explained by pore blockage due to increased metal loadings.

Adsorption−desorption isotherms and the pore-size distributions of fresh Pt/C, Re/C, and PRC12 are compared in Figure 1.

All catalysts displayed isotherms of type I and hysteresis type H4, characteristic of activated carbon, indicating the presence of micropores.[42] The main pore contribution obtained by NL-DFT (Figure 1b) was ca. 0.6 nm for all catalysts.

The decrease in the surface area for spent catalysts was not significant (Figure 2a). Pore-size distribution (Figure 2b) showed no changes in the pore diameter between the fresh and spent catalysts.

Transmission electron micrographs allowed to determine the metal particle sizes of monometallic and bimetallic catalysts (Figure 3, Figure 4). All catalysts exhibited metal particle sizes in the range of 1−2 nm.

The average number-weighted particle sizes for the catalyst were as follows: 2 nm for Pt/C, 1−2 nm for Re/C, 1.9 for PRC21, and 1.5 nm for PRC11. For PRC15 it was not possible to determine the particle sizes, which could be due to smaller not detectable nanoparticles.[43] Moreover, it has been reported that the addition of Re helps in stabilizing other metals in a highly dispersed form on the surface of the support.[44]

TEM micrographs of the spent catalysts (Figure 4) show that there were almost no changes in the metal particle sizes during the reaction. Even after operation at 270 °C (Figure 4b), the particle sizes remained under 2 nm, indicating good stability of metal particles.

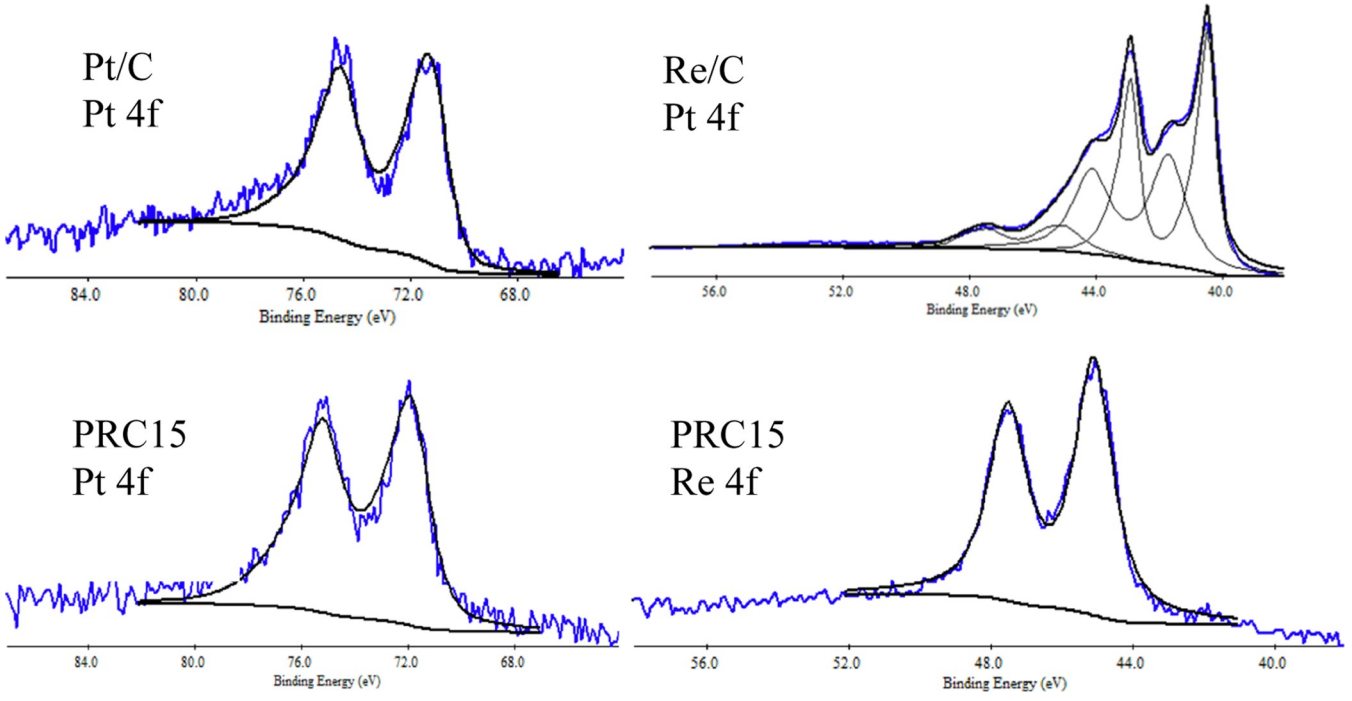

Figure 7. Pt 4f and Re 4f XPS spectra for monometallic Pt/C, Re/C, and bimetallic PRC15 catalysts.

https://doi.org/10.1021/acsengineeringau.2c00015
ACS Eng. Au 2022, 2, 436−449

Table 4. XPS Results for Monometallic Pt/C, Re/C, and Bimetallic PRC15 Catalysts

	Pt/C		Re/C		PRC15		
line	BE[a] (eV)	FWHM (eV)	BE[a] (eV)	FWHM (eV)	BE[a] (eV)	FWHM (eV)	
Pt $4f_{7/2}$	70.99	1.55			71.99	1.66	Pt^0
Re $4f_{7/2}$			40.60	0.96			Re^0
			41.60	0.96			Re^{3+}
			45.08	1	45.11	1.28	Re^{6+}

[a]Shifts in BE values have been normalized with C 1s for these catalysts.

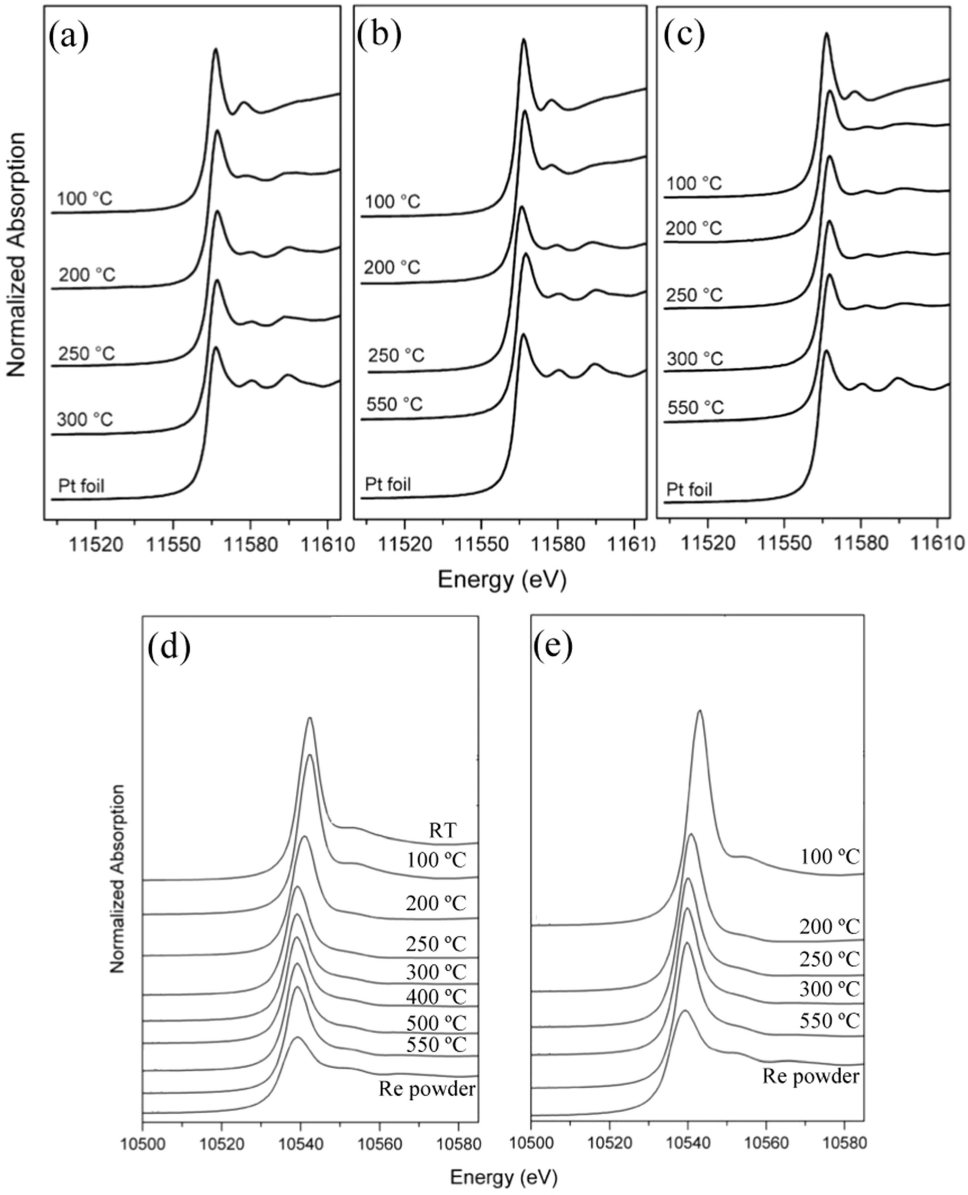

Figure 8. XANES Pt L_{III} edge near-edge spectra of (a) PRC21, (b) PRC11, and (c) PRC15 and Re L_{III} near-edge spectra of (d) PRC12 and (e) PRC15 after reduction at different temperatures. Reprinted with permission from ref 26. Copyright 2014 Elsevier.

NH_3-TPD was performed to obtain information on the acid sites of the catalysts. Pt/C and PRC12 were reduced at 300 °C, while Re/C was reduced at 550 °C. The NH_3-TPD profiles are presented in Figure 5. It should be noted that TPD and ammonia TPD of the bare support resulted in peaks at ca. 150°C of inferior intensity assigned to CO_2 release due to the decomposition of the surface carboxylic groups. Subsequently, desorbed ammonia from the catalysts can be assigned to NH_3 released from the metal phase rather than from the active carbon support.

The higher intensity for the peak observed for PRC12 could be caused by higher dispersion of the metal phase, resulting in more available acid sites, and therefore, more desorbed ammonia. These results are in accordance with microscopy and EXAFS results. The increase of acid sites for bimetallic

https://doi.org/10.1021/acsengineeringau.2c00015
ACS Eng. Au 2022, 2, 436−449

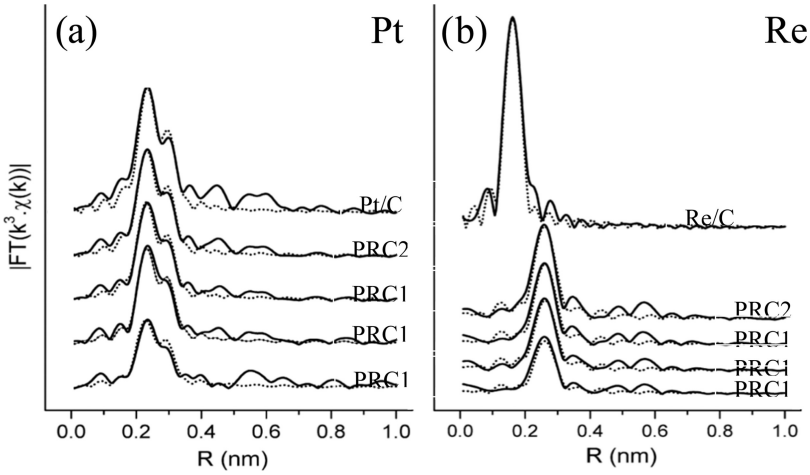

Figure 9. EXAFS spectra Pt L_{III} edge and Re L_{III} edge for monometallic and bimetallic catalysts. Dotted lines represent the fitted spectra. Reprinted with permission from ref 26. Copyright 2014 Elsevier.

Scheme 1. General Reaction Scheme of Hydrodeoxygenation of Isoeugenol

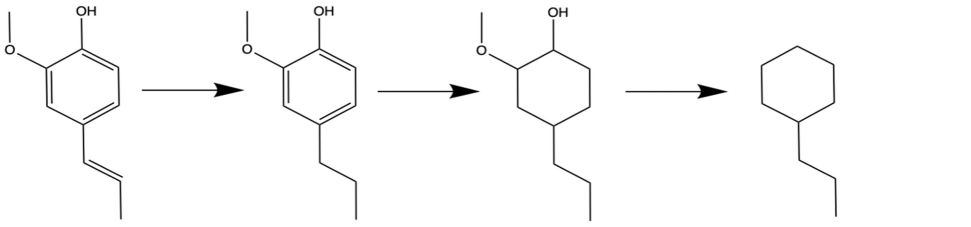

Table 5. Catalytic Activity of Monometallic Pt/C, Re/C, and PRC Catalysts in the Hydrodeoxygenation of Isoeugenol, Performed in a Batch Reactor at 250 °C

entry	catalyst	IE conversion at 4 h (%)[a]	GCLPA (%)[b]	PCH yield (%)	PCH selectivity (%)[c]	HYD yield (%)
1	Pt/C	100 (65)	94	5	4	53
2	Re/C	100 (25)	85	2		8
3	PRC21	100 (98)	53	34	21	24
4	PRC11	100 (98)	54	53	31	11
5	PRC12	100 (100)	71	93	51	0
6	PRC15	100 (100)	77	99	56	0

[a]Conversion of DH in parenthesis (DH *X*). [b]GCLPA (gas chromatography liquid-phase analysis) is an approximation for the mass balance in the liquid phase. [c]Selectivity at 60% DH conversion.

catalysts can also help explain the presence of ReOx, which has been found to be important for deoxygenation.[17]

Reduction profiles for monometallic and bimetallic catalysts were determined by TPR (Figure 6 and Table 3). Reduction peaks for Pt supported on activated carbon have been reported in the 150−300 °C range,[45] for Re it was between 250 and 450 °C.[46] Furthermore, shifts in the reduction peaks have been reported due to the formation of the Pt−Re alloy.[47,48] Additionally, migration of ReOx species toward Pt^0 has also been reported, which can be a result of weak interactions between the metal and the carbon support.[49]

The TPR profile of the activated carbon support displays a peak at ca. 725 °C, observed also for all other samples. This peak has been attributed to the reduction of functional groups on the surface and formation of methane due to interactions between the support and hydrogen.[49,50]

For monometallic catalysts, the reduction profile of Pt/C shows two broad signals below 400 °C (Pt^{4+} to Pt^0), while Re/C reduction displays a pronounced peak at ca. 375 °C (Re^{7+} to Re^0).[49] All PRC catalysts presented a single reduction peak at around 240 °C.

From the TPR profiles, it can be observed that the total amount of consumed H_2 is the lowest for Pt/C. Lower reduction temperatures for bimetallic PRC, when compared to Re/C, indicate that Pt facilitates the reduction of Re,[49] which could be due to hydrogen spillover from Pt^0 to ReOx,[46,51−53] however, a clear signal for Re reduction could not be observed.

The H_2/M ratio was determined by the amount of H_2 consumed per total moles of Pt and Re. The H_2/M ratio (Table 3) is higher than 2 for Pt/C, which could be caused by the reduction of surface oxygen groups of the support. The H_2/M ratio decreases as the Re/Pt ratio increases. High H_2/M values indicate that more H_2 is needed to reduce Re.

X-ray photoelectron spectroscopy (XPS) was performed to determine the electronic states of Pt and Re on the surface of reduced monometallic Pt/C, Re/C, and PRC15 catalysts (Figure 7 and Table 4). The binding energy (BE) values have been normalized to that of C 1s (284.5 eV) for all catalysts. XPS spectra for monometallic Pt/C showed a doublet for Pt $4f_{7/2}$ with the binding energy (BE) of 70.99 eV assigned to Pt^0, which is consistent with the BE values reported in the literature.[54] The same Pt $4f_{7/2}$ doublet assigned to Pt^0 could be observed at the BE of 70.90 eV for the PRC15 catalyst.

https://doi.org/10.1021/acsengineeringau.2c00015
ACS Eng. Au 2022, 2, 436−449

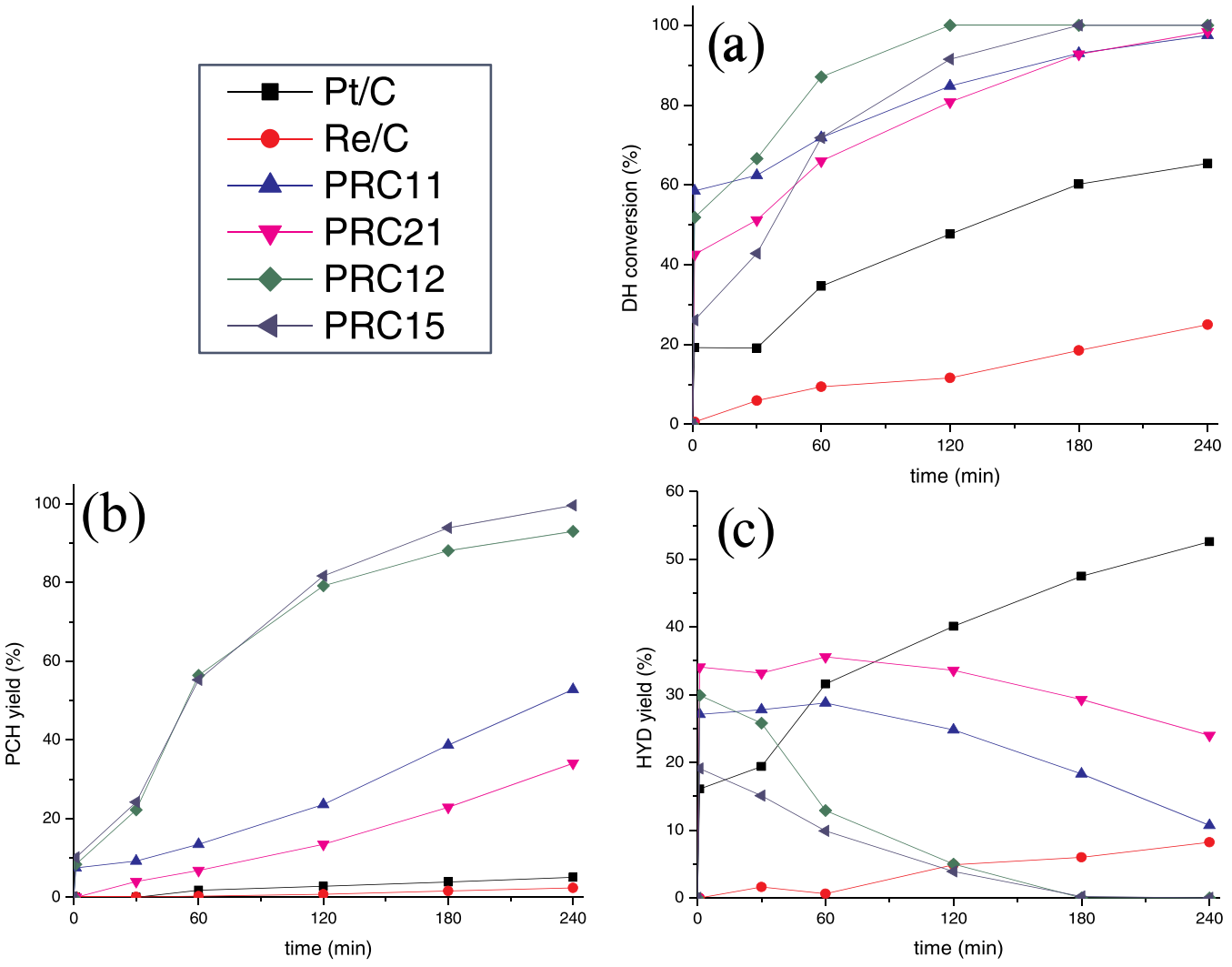

Figure 10. (a) Conversion of dihydroeugenol, (b) yield of propylcyclohexane, and (c) yield of hydrogenated intermediate as a function of time. Conditions: 250 °C and 30 bar of H_2.

XPS spectra for monometallic Re/C showed mixed oxidation states; namely, Re $4f_{7/2}$ binding energy of 40.6 eV was assigned to Re^0, a binding energy of 41.6 eV was assigned to Re^{3+}, while the binding energy of 45.07 eV corresponds to Re^{6+}. Bimetallic PRC15 spectra displayed a doublet signal for Re 4f with a binding energy of 45.02 eV, indicating that Re^{6+} was the predominant species. These values are also consistent with the literature.[54,55] It's important to note that the measurements were performed *ex situ*, and as rhenium is highly oxophilic;[63] its oxidation state could be influenced by exposure to air.

XANES provided a better understanding of the reduction behavior of the catalysts. Figure 8 displays the XANES Pt L_{III} edge near-edge spectra of PRC21, PRC11, and PRC15 and Re LIII near-edge spectra of PRC12 and PRC15 after reduction at different temperatures.

Changes between 200 and 550 °C are small for Pt L_{III} spectra, indicating that Pt reduction mainly occurs between 100 and 200 °C. For PRC15 (Figure 8c), the edge position shifts to higher energy values than Pt foil and reduced Pt/C, implying that Re influenced the electronic structure of Pt.[56]

A shift to lower energies is observed in Re L_{III} XANES spectra of PRC12 and PRC15 (Figure 8d,e). A comparison of the spectra from 100 to 550 °C reveals that Re reduction occurs at higher temperatures, as the spectra display only a minor shift toward lower energy between 250 and 550 °C, which could indicate a partial reduction at these temperatures.[57] XANES spectra of PRC15 are consistent with those of XPS and TPR, showing that a significant amount of Re is found as oxide species when reduced at 350 °C.[43,58,59]

Fourier transform (FT) EXAFS spectra for the catalysts at the Pt L_{III} edge after reduction at 300 °C are presented in Figure 9a. The backscattering functions of Pt and Re were very similar, making the determination between Pt bound to Re or Pt challenging.[60] For bimetallic catalysts, the absence of a Pt−O shell indicates that Pt is reduced at 300 °C. The coordination number (CN) of the Pt−M shell increases with increasing reduction temperature due to the increase in the size or ordering of particles. An increase in the Pt/Re ratio resulted in a decrease of the CN for the Pt−M shell. These results explain the decrease in metal particle sizes with increasing Re content. Furthermore, the Pt−M coordination distance becomes smaller with increasing Re content.

EXAFS results at the Re L_{III} edge (Figure 9b) indicate that Re in Re/C is present mainly as an oxide after reduction at 250 °C, while at 550 °C it is mostly metallic Re and a small portion

https://doi.org/10.1021/acsengineeringau.2c00015
ACS Eng. Au 2022, 2, 436−449

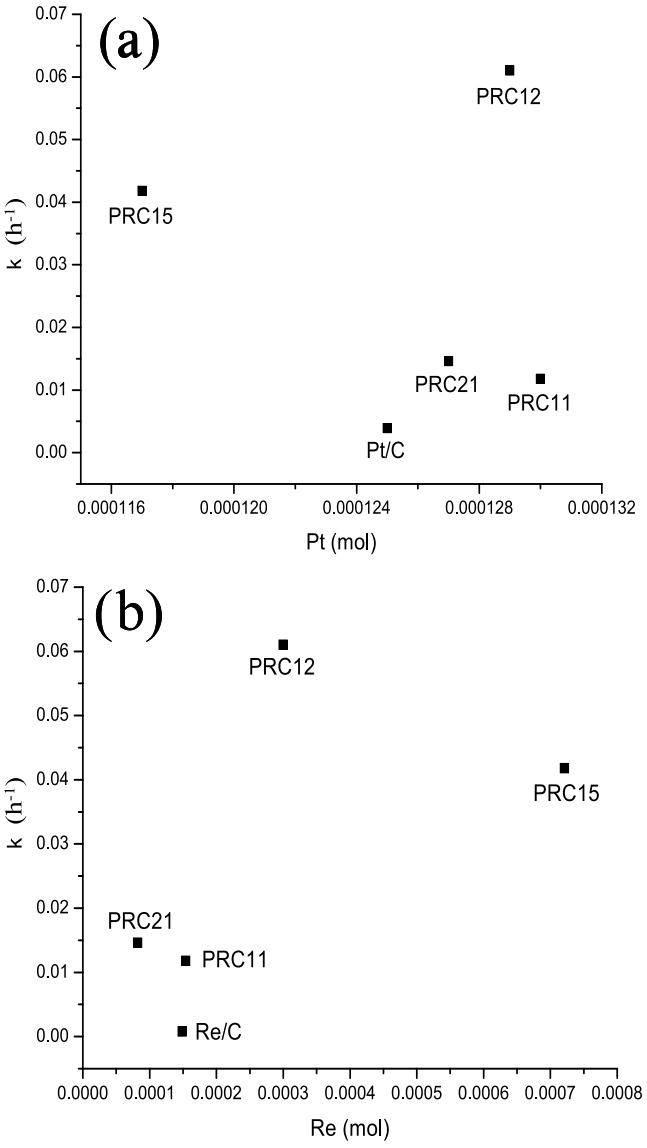

Figure 11. (a) Activity as a function of the amount of Pt (mol) and (b) activity as a function of the amount of Re (mol).

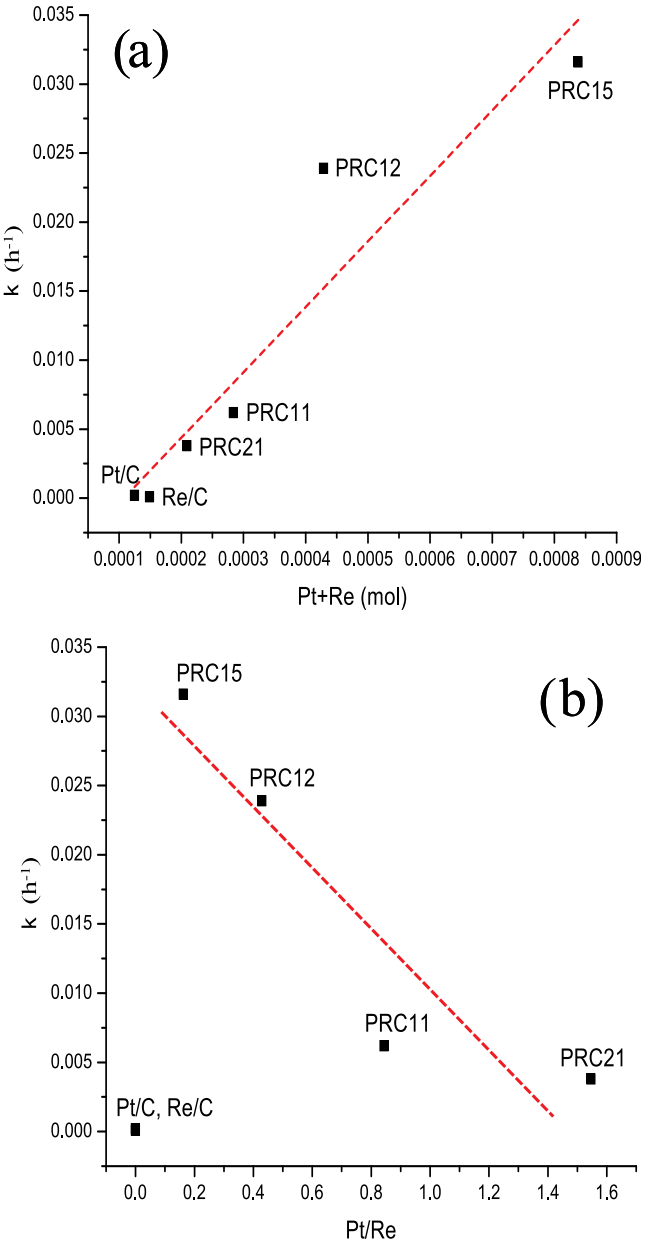

Figure 12. Rate constant as a function of (a) the sum of the Pt and Re content (mol) and (b) the Pt/Re molar ratio.

of ReOx species, which is consistent with the reduction temperature observed for Re/C in TPR (375 °C). For bimetallic catalysts, it was observed that the CN of the Re−M shell increased with the increase of Re loading, this is in accordance with the Pt EXAFS results that explain the decrease in metal particle sizes.

Catalytic Activity

The catalysts were tested for the hydrodeoxygenation (HDO) of isoeugenol (IE) in a batch reactor at temperatures between 230 and 270 °C. The simplified reaction network is presented in Scheme 1.

As reported previously, hydrogenation of the propene group occurs immediately,[61] converting isoeugenol (IE) into dihydroeugenol (DH) in less than 1 min. This is followed by hydrogenation of the aromatic ring, forming 2-methoxy-4-propylcyclohexanol (HYD), which is a hydrogenated intermediate still containing hydroxy and methoxy groups. Their elimination through deoxygenation results in the desired product propylcyclohexane (PCH).

The catalytic results for monometallic and bimetallic catalysts at 250 °C are summarized in Table 5. The main products were 2-methoxy-4-propylcyclohexanol and propylcyclohexane. Time-dependent yields of these compounds are presented in Figure 10.

All catalysts displayed complete isoeugenol conversion (IE *X*) in less than 1 min, therefore, dihydroeugenol conversion (DH *X*) was followed. Data in Figure 10 also illustrate that further transformations of DH started during heating of the reactor or within the 1st min of the reaction, before the first sample is taken, as a substantial conversion of DH is achieved at time zero.

Monometallic catalysts displayed the lowest conversion of DH, 65% for Pt/C (entry 1) and 25% for Re/C (entry 2). Such low values are consistent with those reported in the literature for HDO using monometallic catalysts supported on carbon-type materials.[17] Propylcyclohexane yields (PCH *Y*)

https://doi.org/10.1021/acsengineeringau.2c00015
ACS Eng. Au 2022, 2, 436−449

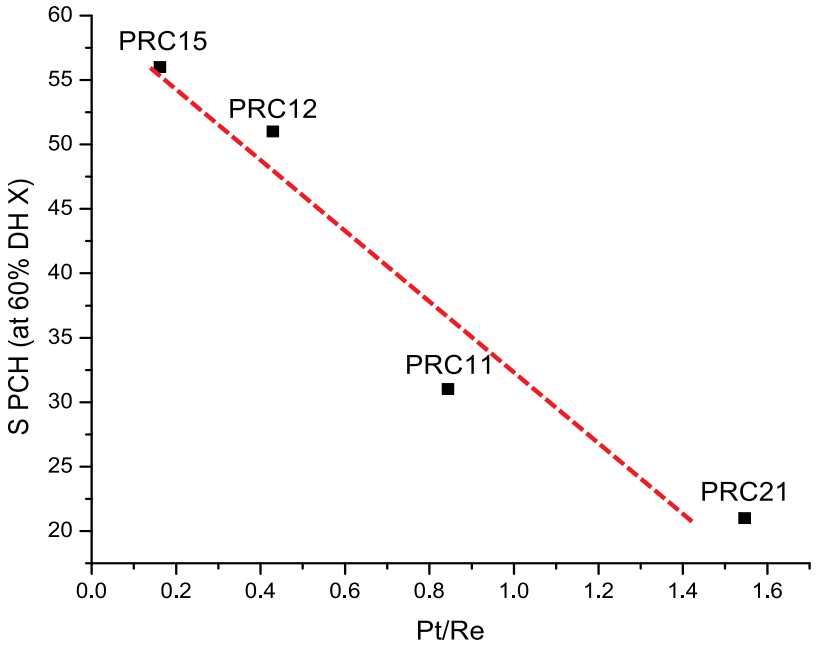

Figure 13. Propylcyclohexane selectivity (at 60% dihydroeugenol conversion) as a function of the Pt/Re molar ratio.

Table 6. Catalytic Activity of PRC15 Catalysts in the Hydrodeoxygenation of Isoeugenol, Performed at 230, 250, and 270 °C

catalyst	temperature (°C)	IE conversion at 4 h (%)[a]	GCLPA (%)[b]	PCH yield (%)	PCH selectivity (%)[c]
PRC15	230	100 (100)	68	88	74.5
PRC15	250	100 (100)	77	99	64.3
PRC15	270	100 (100)	71	92	76.9

[a]Conversion of DH in parenthesis (DH X). [b]GCLPA (gas chromatography liquid-phase analysis) is an approximation for the mass balance in the liquid phase. [c]Selectivity at 80% DH conversion.

were also the lowest for these catalysts, while Pt/C displayed the highest yield of the hydrogenated intermediate (HYD) among all catalysts (Figure 10c). High GCLPA values indicate that most of the products remained in the liquid phase and that deoxygenation/hydrogenolysis was minimal, reflecting relatively low catalytic activity. While gas-phase products were not analyzed, the formation of methanol and H_2O is expected.[62] Subsequently Pt/C and Re/C exhibited mediocre conversion along with high GCLPA.

From these results it can be inferred that while Pt is active in hydrogenating the double bonds from the propenyl group and the aromatic ring, it is not effective in deoxygenation, giving only 5% yield of PCH. Low HYD yields for Re/C (ca. 2%) indicate that rhenium *per se* is not as effective for hydrogenation as Pt/C.

However, for bimetallic catalysts, there was a clear synergetic effect, as all of them exhibited higher catalytic activity than the monometallic catalysts individually, achieving complete DH conversion after 4 h of the reaction time and PCH *Y* >30%. The lowest PCH Y was obtained with PRC21 (entry 3, ca. 35%), the catalyst with the highest Pt/Re ratio. On the other hand, PRC15 displayed the highest PCH Y (entry 6, ca. 99%) and the maximum GCLPA value (77%), indicating almost complete conversion of IE into PCH at 4 h. GCLPA values for PRC catalysts indicate that volatile products were distributed either in the gas phase or in the liquid phase as higher-molecular weight polymers; neither were quantified.

These values seem to indicate that a lower Pt/Re ratio results in higher HDO activity. Furthermore, selectivity toward PCH (normalized at 60% DH conversion) displays the following trend for PRC catalysts: PRC15 > PRC12 > PRC11 > PRC21, indicating that Re plays an important role in hydrodeoxygenation. These results are consistent with the results from XPS, EXAFS, and XANES, as the presence and increase of the ReOx species content resulted in a decrease in the metal particle sizes, and therefore, better dispersion and higher HDO activity. This promotion effect can be explained by the complementarity between the high hydrogenating ability of Pt and the oxophilicity of Re, visible in Figure 11a,b, illustrating that the rate does not depend on the molar content of Pt or Re separately, as no clear trend can be observed.

For these calculations, the reaction was considered to be first-order in DH, while as the pressure was constant and an excess of H_2 of used, the apparent rate constant contains the hydrogen pressure dependence. The rate constant was obtained considering the formation of PCH within 60−240 min time interval. The values for the constant (k) were obtained by linear regression.

On the other hand, when considering both metals, a clear trend of the Pt/Re molar ratio on the rate constant could be identified (Figure 12). A linear increase in activity can be observed proportional to the total amount of Pt and Re (Figure 12a), with monometallic catalysts displaying the lowest activity, and PRC15 the highest. As expected, an increase in the amount of the active phase allows an increase in activity, however, a lower Pt/Re ratio (Figure 12b) also resulted in higher activity and selectivity, leading to a conclusion that both Pt and Re are indispensable to carry out the reaction.

A similar trend as in Figure 12b can be observed in Figure 13, where selectivity toward PCH, the deoxygenated product, is plotted vs the Pt/Re molar ratio. As apparently clear from Figure 13 selectivity is decreasing with an increase of the Pt/Re ratio, highlighting the importance of Re in this catalytic system.

https://doi.org/10.1021/acsengineeringau.2c00015
ACS Eng. Au 2022, 2, 436−449

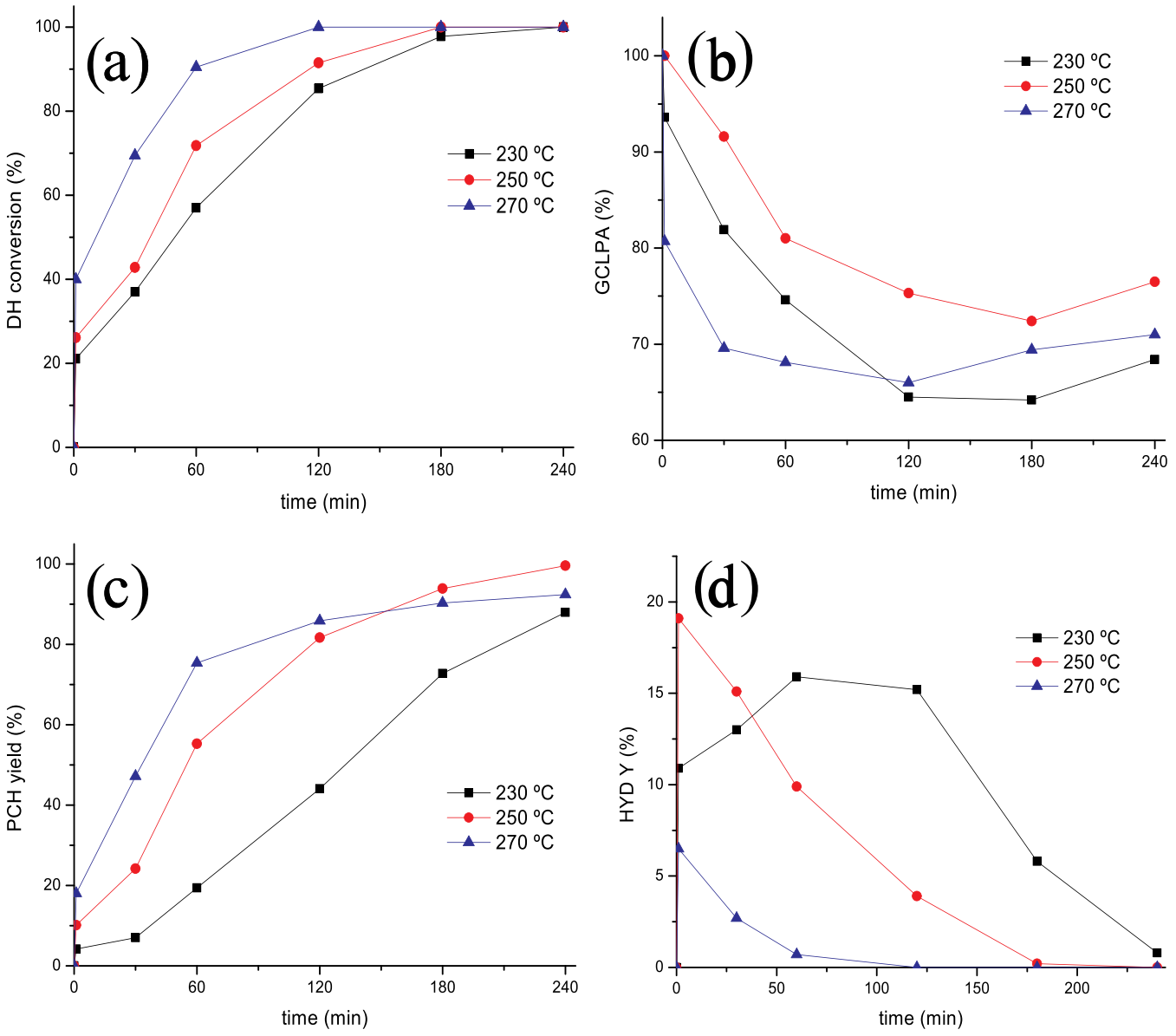

Figure 14. (a) Conversion of dihydroeugenol, (b) GCLPA, (c) PCH Y, and (d) HYD Y for PRC15 at 230, 250, and 270 °C.

For PRC15 and PRC12 catalysts, activity and selectivity toward the deoxygenated product increased, indicating that the deoxygenation route was promoted.

The results of XPS, EXAFS, and XANES reveal the presence of ReOx species when the loading of Re was higher and the particle size was smaller. This can explain the enhanced activity and selectivity toward the deoxygenated product for PRC12 and PRC15 catalysts. Metallic Pt and ReOx have a promotion effect when they are together, improving deoxygenation or breakage of the C−O bond. Similar findings have been reported in the literature, namely, oxophilic oxide in close proximity to a metal particle activates the C−O bond, promoting deoxygenation.[63]

Activation energy was calculated for the HDO of isoeugenol with PRC15 from experiments conducted at 230−270 °C (Table 6 and Figure 14).

The liquid-phase mass balance (GCLPA, Figure 13b) was ca. 70% at 4 h for all temperatures, indicating that majority of the products remained in the liquid phase.

The PCH yield (Figure 14c) was the highest (ca. 99%) at 250 °C, even if the initial PCH yield values were higher at 270 °C. Simultaneously, the yield of HYD (Figure 14d) was the highest at 230 °C, which can be a consequence of stronger catalyst deactivation at a higher temperature. After 4 h only trace amounts of HYD were obtained (<1%). Overall, the highest PCH selectivity (at 80% conversion of DH) was obtained at 270 °C.

The apparent activation energy was calculated for the transformations of dihydroeugenol using experiments at 230, 250, and 270 °C. For this purpose, the reaction was considered as the first-order reaction for DH because of the constant pressure of H_2 also being in excess, the reaction order toward hydrogen is zero. Additionally, only the time between 1 and 120 min was considered. The values for the constant (k) were obtained for each temperature by linear regression and then plotted in the Arrhenius coordinates (Figure 15). The apparent activation energy obtained for HDO of IE using PRC15 was 43.7 kJ/mol.

https://doi.org/10.1021/acsengineeringau.2c00015
ACS Eng. Au 2022, 2, 436−449

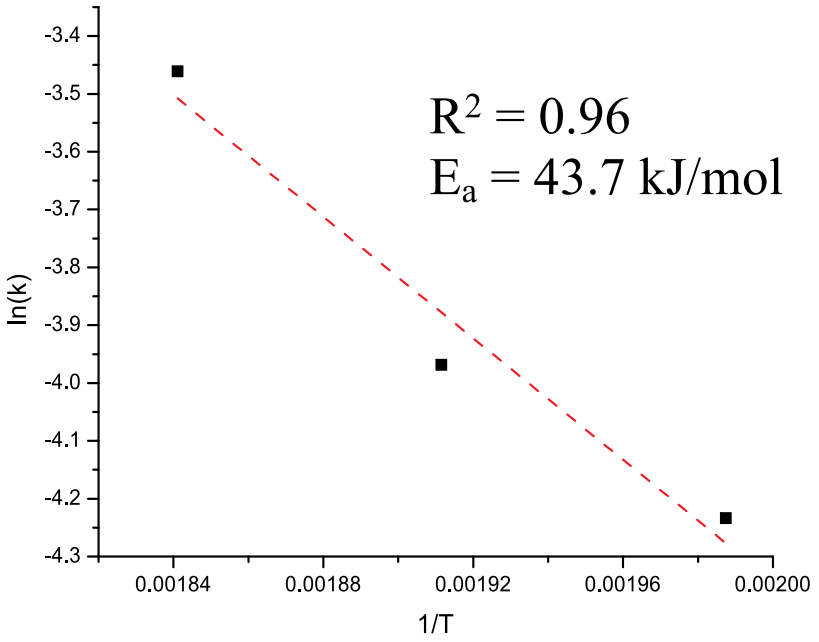

Figure 15. Arrhenius plot for the hydrodeoxygenation of isoeugenol on PRC15.

In our previous work, activation energy for HDO of isoeugenol (15 kJ/mol) was determined in a continuous reactor where mass-transfer limitations were present.[17] The value obtained in this article is of the same magnitude as activation energies for HDO of other phenol-based model compounds reported in the literature.[59,60] The apparent activation energy for ring saturation and hydrodeoxygenation of phenol was ca. 59 kJ/mol, using a Pt/Al_2O_3 catalyst in a batch reactor.[64] HDO of dihydroeugenol using a sulfided NiMo catalyst resulted in an activation energy of ca. 34 kJ/mol in a packed-bed microreactor.[65] DH conversion reached 100% at 4 h for all temperatures. As expected, the fastest DH was achieved at the highest temperature (Figure 14a).

CONCLUSIONS

Bimetallic Pt−Re catalysts supported on microporous activated carbon catalysts displayed high activity for the HDO of isoeugenol. A higher amount of Re resulted in smaller Pt particles, and therefore, higher dispersion. Characterization of the catalysts revealed that after reduction, Pt was present in the metallic state, while Re was predominantly present as ReOx. Regarding catalytic activity, a promotion effect was observed for bimetallic catalysts. Complete conversion of isoeugenol and dihydroeugenol were observed for all bimetallic catalysts, with the yields of the desired product, propylcyclohexane, increasing with the Re content. As such, the Pt−Re catalyst with a Pt/Re atomic ratio of 1/5 was the most active catalyst, achieving 99% propylcyclohexane yield at 4 h and 77% mass balance closure in the liquid phase. Selectivity at 60% of dihydroeugenol conversion was also the highest for the same catalyst (56%).

The most active catalyst exhibited the smallest particle sizes and more ReOx species, verified by XPS, EXAFS, and XANES, which could explain the catalytic performance, as they provide the oxygen vacancies required for the deoxygenation to take place.

The catalyst with a higher Pt/Re ratio (2:1) displayed a decrease in activity (34% propylcyclohexane yield, 21% propylcyclohexane selectivity). Also giving the highest yield (ca. 25%) of the hydrogenated intermediate, 2-methoxy-4-propylcyclohexanol, among all bimetallic catalysts. For this bimetallic system, Pt performed the hydrogenation of double bonds while ReOx was needed to deoxygenate dihydroeugenol. A higher Re content and a lower Pt/Re ratio also had a positive effect on activity.

The apparent activation energy was determined for the first time for HDO of isoeugenol in a batch reactor in a temperature range of 230−270 °C, the value was 43.7 kJ/mol.

AUTHOR INFORMATION

Corresponding Author

Dmitry Yu. Murzin − *Johan Gadolin Process Chemistry Centre, Åbo Akademi University, 20500 Turku/Åbo, Finland*; orcid.org/0000-0003-0788-2643; Email: dmurzin@abo.fi

Authors

Mark Martinez-Klimov − *Johan Gadolin Process Chemistry Centre, Åbo Akademi University, 20500 Turku/Åbo, Finland*

Päivi Mäki-Arvela − *Johan Gadolin Process Chemistry Centre, Åbo Akademi University, 20500 Turku/Åbo, Finland*; orcid.org/0000-0002-7055-9358

Ayşegül Çiftçi − *Laboratory of Inorganic Materials and Catalysis, Department of Chemical Engineering and Chemistry, Eindhoven University of Technology, 5600 MB Eindhoven, The Netherlands*

Narendra Kumar − *Johan Gadolin Process Chemistry Centre, Åbo Akademi University, 20500 Turku/Åbo, Finland*

Kari Eränen − *Johan Gadolin Process Chemistry Centre, Åbo Akademi University, 20500 Turku/Åbo, Finland*

Markus Peurla − *Institute of Biomedicine, University of Turku, 20520 Turku, Finland*

Emiel J. M. Hensen − *Laboratory of Inorganic Materials and Catalysis, Department of Chemical Engineering and Chemistry, Eindhoven University of Technology, 5600 MB Eindhoven, The Netherlands*; orcid.org/0000-0002-9754-2417

https://doi.org/10.1021/acsengineeringau.2c00015
ACS Eng. Au 2022, 2, 436−449

Complete contact information is available at:
https://pubs.acs.org/10.1021/acsengineeringau.2c00015

Notes

The authors declare no competing financial interest.

■ ACKNOWLEDGMENTS

Electron microscopy samples were processed and analyzed in the Electron Microscopy Laboratory, Institute of Biomedicine, University of Turku, which receives financial support from Biocenter Finland. XPS samples were processed and analyzed in the Department of Physics and Astronomy, Quantum Building, University of Turku. The authors acknowledge Sari Granroth and Atte Aho for support in utilizing and analyzing XPS results. This work was supported by the Magnus Ehrnrooth Foundation.

■ REFERENCES

(1) Markard, J. The Next Phase of the Energy Transition and its Implications for Research and Policy. *Nat. Energy* **2018**, *3*, 628−633.
(2) Horn, R. A. *Morphology of Wood Pulp Fiber from Softwoods and Influence on Paper Strength. Research Paper FPL-242*; Department of Agriculture, Forest Service, Forest Products Laboratory: Madison, WI, USA, 1974.
(3) Miura, M.; Shimotori, Y.; Nakatani, H.; Harada, A.; Aoyama, M. Bioconversion of Birch Wood Hemicellulose Hydrolyzate to Xylitol. *Appl. Biochem. Biotechnol.* **2015**, *176*, 947−955.
(4) Delbecq, F.; Wang, Y.; Muralidhara, A.; El Ouardi, K.; Marlair, G.; Len, C. Hydrolysis of Hemicellulose and Derivatives—A Review of Recent Advances in the Production of Furfural. *Front. Chem.* **2018**, *6*, No. 146.
(5) Abdullah, B.; Muhammad, S. A. F. A. S.; Mahmood, N. A. N. Production of Biofuel via Hydrogenation of Lignin from Biomass. In *New Advances in Hydrogenation Processes - Fundamentals and Applications*, IntechOpen, 2017; pp 289−305.
(6) Schutyser, W.; Renders, T.; Van den Bosch, S.; Koelewijn, S.-F.; Beckham, G. T.; Sels, B. F. Chemicals from Lignin: An Interplay of Lignocellulose Fractionation, Depolymerisation, and Upgrading. *Chem. Soc. Rev.* **2018**, *47*, 852−908.
(7) Sudarsanam, P.; Peeters, E.; Makshina, E. V.; Parvulescu, V. I.; Sels, B. F. Advances in Porous and Nanoscale Catalysts for Viable Biomass Conversion. *Chem. Soc. Rev.* **2019**, *48*, 2366−2421.
(8) Haq, I.; Mazumder, P.; Kalamdhad, A. S. Recent Advances in Removal of Lignin from Paper Industry Wastewater and its Industrial Applications-A Review. *Bioresour. Technol.* **2020**, *312*, No. 123636.
(9) Sun, Z.; Fridrich, B.; de Santi, A.; Elangovan, S.; Barta, K. Bright Side of Lignin Depolymerization: Toward New Platform Chemicals. *Chem. Rev.* **2018**, *118*, 614−678.
(10) Meng, J.; Moore, A.; Tilotta, D.; Kelley, S.; Park, S. Toward Understanding of Bio-Oil Aging: Accelerated Aging of Bio-oil Fractions. *ACS Sustainable Chem. Eng.* **2014**, *2*, 2011−2018.
(11) Mortensen, P. M.; Grunwaldt, J.-D.; Jensen, P. A.; Knudsen, K. G.; Jensen, A. D. A Review of Catalytic Upgrading of Bio-oil to Engine Fuels. *Appl. Catal., A* **2011**, *407*, 1−19.
(12) Mäki-Arvela, P.; Murzin, D. Y. Hydrodeoxygenation of Lignin-Derived Phenols: from Fundamental Studies Towards Industrial Applications. *Catalysts* **2017**, *7*, No. 265.
(13) Laurent, E.; Delmon, B. Study of the Hydrodeoxygenation of Carbonyl, Carboxylic and Guaiacyl Groups over Sulfided CoMo/γ-Al_2O_3 and NiMo/γ-Al_2O_3 Catalysts. *Appl. Catal., A* **1994**, *109*, 77−96.
(14) Ohta, H.; Kobayashi, H.; Hara, K.; Fukuoka, A. Hydrodeoxygenation of Phenols as Lignin Models under Acid-Free Conditions with Carbon-Supported Platinum Catalysts. *Chem. Commun.* **2011**, *47*, 12209.
(15) Vasilevich, A. V.; Baklanova, O. N.; Lavrenov, A. V. Hydrodeoxygenation of Guaiacol with Molybdenum-Carbide-Based Carbon Catalysts. *ChemistrySelect* **2020**, *5*, 4575−4579.
(16) Jung, K. B.; Lee, J.; Ha, J.-M.; Lee, H.; Suh, D. J.; Jun, C.-J.; Jae, J. Effective Hydrodeoxygenation of Lignin-Derived Phenols using Bimetallic RuRe Catalysts: Effect of Carbon Supports. *Catal. Today* **2018**, *303*, 191−199.
(17) Martínez-Klimov, M. E.; Mäki-Arvela, P.; Vajglova, Z.; Alda-Onggar, M.; Angervo, I.; Kumar, N.; Eränen, K.; Peurla, M.; Calimli, M. H.; Muller, J.; Shchukarev, A.; Simakova, I. L.; Murzin, D. Y. Hydrodeoxygenation of Isoeugenol over Carbon-Supported Pt and Pt-Re Catalysts for Production of Renewable Jet Fuel. *Energy Fuels* **2021**, *35*, 17755−17768.
(18) Lu, M.; Du, H.; Wei, B.; Zhu, J.; Li, M.; Shan, Y.; Song, C. Catalytic Hydrodeoxygenation of Guaiacol over Palladium Catalyst on Different Titania Supports. *Energy Fuels* **2017**, *31*, 10858−10865.
(19) Mäkelä, E.; González Escobedo, J. L.; Lindblad, M.; Käldström, M.; Meriö-Talvio, H.; Jiang, H.; Puurunen, R. L.; Karinen, R. Hydrodeoxygenation of Levulinic Acid Dimers on a Zirconia-Supported Ruthenium Catalyst. *Catalysts* **2020**, *10*, No. 200.
(20) Afrin, S.; Bollini, P. Cerium Oxide Catalyzes the Selective Vapor Phase Hydrodeoxygenation of Anisole to Benzene at Ambient Pressures of Hydrogen. *Ind. Eng. Chem. Res.* **2019**, *58*, 14603−14607.
(21) Chen, M.-Y.; Huang, Y.-B.; Pang, H.; Liu, X.-X.; Fu, Y. Hydrodeoxygenation of Lignin-Derived Phenols into Alkanes over carbon Nanotube Supported Ru Catalysts in Biphasic Systems. *Green Chem.* **2015**, *17*, 1710−1717.
(22) Vargas-Villagrán, H.; Flores-Villeda, M. A.; Puente-Lee, I.; Solís-Casados, D. A.; Gómez-Cortés, A.; Díaz-Guerrero, G.; Klimova, T. E. Supported Nickel Catalysts for Anisole Hydrodeoxygenation: Increase in the Selectivity to Cyclohexane. *Catal. Today* **2018**, *341*, 26−41.
(23) Guan, Q.; Wan, F.; Han, F.; Liu, Z.; Li, W. Hydrodeoxygenation of Methyl Palmitate over MCM-41 Supported Nickel Phosphide Catalysts. *Catal. Today* **2016**, *259*, 467−473.
(24) Martínez-Klimov, M. E.; Mäki-Arvela, P.; Murzin, D. Y. Catalysis for Production of Jet Fuel from Renewable Sources by Hydrodeoxygenation and Hydrocracking. In *Catalysis*, RSC, 2021; Vol. *33*, pp 181−213.
(25) Burch, R. The Oxidation State of Rhenium and Its Role in Platinum-Rhenium Reforming Catalysts. *Platinum Met. Rev.* **1978**, *22*, 57−60.
(26) Ciftci, A.; Ligthart, D. A. J. M.; Sen, A. O.; van Hoof, A. J. F.; Friedrich, H.; Hensen, E. J. M. Pt-Re Synergy in Aqueous-Phase Reforming of Glycerol and the Water-gas Shift Reaction. *J. Catal.* **2014**, *311*, 88−101.
(27) Sakkas, P. M.; Argirusi, M.; Sourkouni, G.; Argirusis, C. Rhenium Oxide Nanoparticles − Sonochemical Synthesis and Integration on Anode Powders for Solid Oxide Fuel Cells. *Ultrason. Sonochem.* **2020**, *69*, No. 105250.
(28) Jüntgen, H. Activated carbon as catalyst support. *Fuel* **1986**, *65*, 1436−1446.
(29) Dowaidar, A. M.; El-Shahawi, M. S.; Ashour, I. Adsorption of Polycyclic Aromatic Hydrocarbons onto Activated Carbon from Non-Aqueous Media: 1. The Influence of the Organic Solvent Polarity. *Sep. Sci. Technol.* **2007**, *42*, 3609−3622.
(30) Sarioğlan, Ş. Recovery of Palladium from Spent Activated Carbon-Supported Palladium Catalysts. *Platinum Met. Rev.* **2013**, *57*, 289−296.
(31) Berenguer, A.; Sankaranarayanan, T. M.; Gómez, G.; Moreno, I.; Coronado, J. M.; Pizarro, P.; Serrano, D. P. Evaluation of Transition Metal Phosphides Supported on Ordered Mesoporous Materials as Catalysts for Phenol Hydrodeoxygenation. *Green Chem.* **2016**, *18*, 1938−1951.
(32) Sulman, A.; Mäki-Arvela, P.; Bomont, L.; Alda-Onggar, M.; Fedorov, V.; Russo, V.; Eränen, K.; Peurla, M.; Akhmetzyanova, U.; Skuhrovcová, L.; Tišler, Z.; Grénman, H.; Wärnå, J.; Murzin, D. Y. Kinetic and Thermodynamic Analysis of Guaiacol Hydrodeoxygenation. *Catal. Lett.* **2019**, *149*, 2453−2467.
(33) Gao, D.; Xiao, Y.; Varma, A. Guaiacol Hydrodeoxygenation over Platinum Catalyst: Reaction Pathways and Kinetics. *Ind. Eng. Chem. Res.* **2015**, *54*, 10638−10644.

(34) Santos, J. L.; Alda-Onggar, M.; Fedorov, V.; Peurla, M.; Eränen, K.; Mäki-Arvela, P.; Centeno, M. Á.; Murzin, D. Y. Hydrodeoxygenation of Vanillin Over Carbon Supported Metal Catalysts. *Appl. Catal., A.* **2018**, *561*, 137−149.
(35) Lyu, G.; Wu, S.; Zhang, H. Estimation and Comparison of Bio-Oil Components from Different Pyrolysis Conditions. *Front. Energy Res.* **2013**, *3*, No. 28.
(36) Duval, A.; Lawoko, M. A. Review on Lignin-Based Polymeric, Micro- and Nano-structured Materials. *React. Funct. Polym.* **2014**, *85*, 78−96.
(37) Hileman, J. I.; Stratton, R. W. Alternative Jet Fuel Feasibility. *Transp. Policy* **2014**, *34*, 52−62.
(38) Kallio, P.; Pásztor, A.; Akhtar, M. K.; Jones, P. R. Renewable Jet Fuel. *Curr. Opin. Biotechnol.* **2014**, *26*, 50−55.
(39) Markard, J. The Next Phase of the Energy Transition and its Implications for Research and Policy. *Nat. Energy* **2018**, *3*, 628−633.
(40) Kammermann, J.; Bolvashenkov, I.; Tran, K.; Herzog, H. -G.; Frenkel, I. In *Feasibility Study for a Full-Electric Aircraft Considering Weight, Volume, and Reliability Requirements*, International Conference on Electrotechnical Complexes and Systems (ICOECS), 2020; pp 1−6.
(41) Hu, X.; Gholizadeh, M. Progress of the Applications of Bio-Oil. *Renewable Sustainable Energy Rev.* **2020**, *134*, No. 110124.
(42) Leofanti, G.; Padovan, M.; Tozzola, G.; Venturelly, B. Surface Area and Pore Texture of Catalysts. *Catal. Today* **1998**, *41*, 207−219.
(43) Dexpert, H.; Lagarde, P.; Bournonville, J. P. Exafs Studies of Bimetallic Pt-Re/Al_2O_3 Catalysts. *J. Mol. Catal.* **1984**, *25*, 347−355.
(44) Yentekakis, I. V.; Goula, G.; Panagiotopoulou, P.; Kampouri, S.; Taylor, M. J.; Kyriakou, G.; Lambert, R. M. Stabilization of Catalyst Particles Against Sintering on Oxide Supports with High Oxygen Ion Lability Exemplified by Ir- Catalyzed Decomposition of N_2O. *Appl. Catal., B* **2016**, *192*, 357−364.
(45) Chen, N.-Y.; Liu, M.-C.; Yang, S.-C.; Chang, J.-R. EXAFS Peaks and TPR Characterizing Bimetallic Interactions: Effects of Impregnation Methods on the Structure of Pt-Ru/C Catalysts. *J. Spectrosc.* **2014**, *34*, No. 347078.
(46) Di, X.; Li, C.; Lafaye, G.; Especel, C.; Epron, F.; Liang, C. Influence of Re−M Interactions in Re−M/C Bimetallic Catalysts Prepared by a Microwave-Assisted Thermolytic Method on Aqueous-Phase Hydrogenation of Succinic Acid. *Catal. Sci. Technol.* **2017**, *7*, 5212−5223.
(47) Iida, H.; Igarashi, A. Structure Characterization of Pr-Re/TiO_2 (Rutile) and Pt-Re/ZrO_2 Catalysts for Water gas Shift Reaction at Low-temperature. *Appl. Catal., A* **2006**, *303*, 192−198.
(48) Iida, H.; Igarashi, A. Difference in the Reaction Behavious Between Pt-Re/TiO_2 (Rutile) and Pt-Re/ZrO_2 Catalysts for Low-Temperature Water Gas Shift Reactions. *Appl. Catal., A* **2006**, *303*, 48−55.
(49) Simonetti, D.; Kunkes, E.; Dumesic, J. Gas-Phase Conversion of Glycerol to Synthesis Gas over Carbon-Supported Platinum and Platinum−Rhenium Catalysts. *J. Catal.* **2007**, *247*, 298−306.
(50) Azzam, K. G.; Babich, I. V.; Seshan, K.; Lefferts, L. A Bifunctional Catalyst for the Single-stage Water-gas Shift Reaction in Fuel Cell Applications. Part 2. Roles of the Support and Promoter on Catalyst Activity and Stability. *J. Catal.* **2007**, *251*, 163−171.
(51) Conner, W. C.; Falconer, J. L. Spillover in Heterogeneous Catalysis. *Chem. Rev.* **1995**, *95*, 759−788.
(52) Prins, R. Hydrogen Spillover. Facts and Fiction. *Chem. Rev.* **2012**, *112*, 2714−2738.
(53) Nakagawa, Y.; Tazawa, S.; Wang, T.; Tamura, M.; Hiyoshi, N.; Okumura, K.; Tomishige, K. Mechanistic Study of Hydrogen-Driven Deoxydehydration over Ceria-Supported Rhenium Catalyst Promoted by Au Nanoparticles. *ACS Catal.* **2018**, *8*, 584−595.
(54) Moulder, J. F.; Stickle, W. F.; Sobol, P. E.; Bomben, K. D. In *Handbook of X-ray Photoelectron Spectroscopy*, Chastain, J., Ed.; Perkin Elmer, 1992.
(55) Takeda, Y.; Tamura, M.; Nakagawa, Y.; Okumura, K.; Tomishige, K. Characterization of Re-Pd/SiO_2 Catalysts for Hydrogenation of Stearic Acid. *ACS Catal.* **2015**, *5*, 7034−7047.
(56) Sá, J.; Kartusch, C.; Makosch, M.; Paun, C.; van Bokhoven, J. A.; Kleymenov, E.; Szlachetko, J.; Nachtegaal, M.; Manyar, H. G.; Hardacre, C. Evaluation of Pt and Re Oxidation State in a Pressurized Reactor: Difference in Reduction Between Gas and Liquid Phase. *Chem. Commun.* **2011**, *47*, 6590−6592.
(57) Tougerti, A.; Cristol, S.; Berrier, E.; Briois, V.; La Fontaine, C.; Villain, F.; Joly, Y. XANES Study of Rhenium Oxide Compounds at the L1 and L3 Absorption Edges. *Phys. Rev. B* **2012**, *85*, No. 125136.
(58) Xiao, J. L.; Puddephatt, R. J. Pt-Re Clusters and Bimetallic Catalysts. *Coord. Chem. Rev.* **1995**, *143*, 457−500.
(59) Ebashi, T.; Ishida, Y.; Nakagawa, Y.; Ito, S.; Kubota, T.; Tomishige, K. Preferential CO Oxidation in a H_2-Rich Stream on Pt-ReOx/SiO2: Catalyst Structure and Reaction Mechanism. *J. Phys. Chem. C* **2010**, *114*, 6518−6526.
(60) Ma, L.; He, D. H.; Li, Z. P. Promoting Effect of Rhenium on Catalytic Performance of Ru Catalysts in Hydrogenolysis of Glycerol to Propanediol. *Catal. Commun.* **2008**, *9*, 2489−2495.
(61) Lindfors, C.; Mäki-Arvela, P.; Paturi, P.; Aho, A.; Eränen, K.; Hemming, J.; Peurla, M.; Kubicka, D.; Simakova, I. L.; Murzin, D. Y. Hydrodeoxygenation of Isoeugenol Over Ni- and Co-Supported Catalysts. *ACS Sustainable Chem. Eng.* **2019**, *7*, 14545−14560.
(62) Teles, C. A.; Rabelo-Neto, R. C.; Duong, N.; Quiroz, J.; Camargo, P. H.; Jacobs, G.; Resasco, D. E.; Noronha, F. B. Role of the Metal-Support Interface in the Hydrodeoxygenation Reaction of Phenol. *Appl. Catal., B* **2020**, *277*, No. 119238.
(63) Bomont, L.; Alda-Onggar, M.; Fedorov, V.; Aho, A.; Peltonen, J.; Eränen, K.; Peurla, M.; Kumar, N.; Wärnå, J.; Russo, V.; Mäki-Arvela, P.; Grénman, H.; Lindblad, M.; Murzin, D. Y. Production of Cycloalkanes in Hydrodeoxygenation of Isoeugenol over Pt- and Ir-Modified Bifunctional Catalysts. *Eur. J. Inorg. Chem.* **2018**, *2018*, 2841−2854.
(64) Funkenbusch, L. T.; Mullins, M. E.; Salam, M. A.; Creaser, D.; Olsson, L. Catalytic Hydrotreatment of Pyrolysis Oil Phenolic Compounds over Pt/Al_2O_3 and Pd/C. *Fuel* **2019**, *243*, 441−448.
(65) Joshi, N.; Lawal, A. Hydrodeoxygenation of 4-Propylguaiacol (2-Methoxy-4-propylphenol) in a Microreactor: Performance and Kinetic Studies. *Ind. Eng. Chem. Res.* **2013**, *52*, 4049−4058.

https://doi.org/10.1021/acsengineeringau.2c00015
ACS Eng. Au 2022, 2, 436−449